scientific reports

OPEN

Theoretical analysis of low power optogenetic control of synaptic plasticity with subcellular expression of CapChR2 at postsynaptic spine

Nripesh Dixit, Gur Pyari, Himanshu Bansal & Sukhdev Roy✉

Precise control of intracellular calcium (Ca^{2+}) concentration at the synaptic neuron terminal can unravel the mechanism behind computation, learning, and memory formation inside the brain. Recently, the discovery of Ca^{2+}-permeable channelrhodopsins (CapChRs) has opened the opportunity to effectively control the intracellular Ca^{2+} concentration using optogenetics. Here, we present a new theoretical model for precise optogenetic control with newly discovered CapChR2 at postsynaptic neuron. A detailed theoretical analysis of coincident stimulation of presynaptic terminal, postsynaptic spine and optogenetic activation of CapChR2-expressing postsynaptic spine shows different ways to control postsynaptic intracellular Ca^{2+} concentration. Irradiance-dependent Ca^{2+} flow is an additional advantage of this novel method. The minimum threshold of light irradiance and optimal ranges of time lag among different stimulations and stimulation frequencies have also been determined. It is shown that synaptic efficacy occurs at 20 μW/mm^2 at coincident electrical stimulation of presynaptic terminal and postsynaptic spine with optogenetic activation of CapChR2-expressed postsynaptic spine. The analysis provides a new means of direct optogenetic control of Ca^{2+}-based synaptic plasticity, better understanding of learning and memory processes, and opens prospects for targeted therapeutic interventions to modulate synaptic function and address various neurological disorders.

Keywords Optogenetics, Neurotransmitter, Intracellular calcium concentration, CapChR2, Synaptic efficacy

Calcium $\left(Ca^{2+}\right)$ ions play a pivotal role in synaptic plasticity, a fundamental process for learning and memory in the brain[1]. The communication between neurons at the chemical synaptic cleft is initiated with the influx of Ca^{2+} due to the release of neurotransmitters from synaptic vesicles at presynaptic terminal[2]. Binding of these neurotransmitters at the specific receptors at the postsynaptic spine increases the intracellular postsynaptic Ca^{2+} levels. This elevated Ca^{2+} level acts as a crucial secondary messenger for initiating a cascade of molecular events that include gene transcription, protein synthesis, or remodeling of the actin cytoskeleton[1]. These processes contribute to synaptic plasticity and lead to long-term changes in the synaptic strength[3,4]. Optimal synaptic communication is essential for the proper brain physiology and slight perturbations of synaptic function can lead to brain disorders. A recent study has demonstrated the relevance of synapse dysfunction as a major determinant of many neurological diseases[5]. Hence, precise spatiotemporal control of Ca^{2+} influx is crucial for optimal synaptic transmission, and helpful to unravel the molecular mechanisms that govern the adaptive changes in neuronal connections. It provides insights into the basis of learning and memory in the intricate network of the nervous system[4].

Optogenetics has revolutionized the field of neuroscience and cell biology by providing the ability to control and monitor the activity of genetically modified cells in tissue culture and living animals with light at unprecedented spatiotemporal resolution[6,7]. It has a wide range of applications in and beyond neuroscience with the first successful human clinical trial of vision restoration reported in 2021[8]. Most early optogenetic experiments involved the expression of light-sensitive proteins throughout the cell structure[9]. Hence, the

Department of Physics and Computer Science, Dayalbagh Educational Institute, Agra 282005, India. ✉email: sukhdevroy@dei.ac.in

context-dependent effects of highly localized intracellular signaling events are not often reflected. Recently, efforts have been made to develop subcellular targeting of light-sensitive proteins to achieve compartment-specific opsin-expression[10]. Such subcellular expression strategies and advanced light delivery technologies open opportunities to target dendrites and synapses, thereby providing means to unravel the mechanism behind logic, memory, learning, and computation.

Channelrhodopsin-2 (ChR2), a non-selective light-gated ion channel, is one of the most used opsins in optogenetics[11,12]. In ChR2-expressing neurons, light stimulation results in the influx of positive ions through these channels, leading to an action potential (AP)[13,14]. Earlier, optogenetic two-photon Ca^{2+} imaging of neurons exhibited significantly larger Ca^{2+} transients in dendrites and spines than with brief somatic current injection[15]. Hence, light-evoked APs result in a very high probability of neurotransmitter release, which leads to a change in synaptic efficacy[16]. However, on clamping the neuron at -65 mV, there is no Ca^{2+} influx, indicating that the natural voltage-gated Ca^{2+} channels are the main contributors to the Ca^{2+} influx. It has also been reported that ChR2 pores do not have any measurable contribution in this Ca^{2+} influx[14]. This is due to low conductance and poor permeability for Ca^{2+} ions through ChR2, which limits its application for efficiently triggering Ca^{2+}-based signaling neurotransmission at the synapse[14,15]. Recent efforts have been made to develop alternative optogenetic methods and tools for controlling synaptic plasticity. These methods include control of neurotransmitter release at presynaptic neuron, presynaptic potentiation with light, presynaptic organelles and proteins, and AMPA receptor endocytosis process[16,17].

Recently, Ca^{2+}-permeable channelrhodopsins (CapChRs) have been discovered through targeted mutagenesis[9]. The two mutants of CapChR, namely CapChR1 and CapChR2 exhibit improved strong permeability for Ca^{2+} at negative voltage and low extracellular Ca^{2+} concentrations[9]. Optogenetic excitation of CapChR2, a mutant with higher Ca^{2+} permeability, reliably increases intracellular Ca^{2+} concentrations in cultured neurons and robustly triggers Ca^{2+} signaling[9]. Therefore, CapChR2 would be suitable for the optical dissection of different Ca^{2+}-dependent processes that have yet to be understood completely. Furthermore, localized expression of these Ca^{2+} conducting channels at the synaptic spines may allow effective control of synaptic plasticity.

Computational models are essential in neuroscience as they provide a deeper understanding of ionic transportation across the cell membrane. Earlier reported computational models for optogenetic control of neurons at cell, circuit, and network levels have significantly improved the understanding of how light-evoked ionic currents through ChRs can lead to AP[18,19]. The intricate dynamics exhibited by single or multiple opsin-expressing neurons in response to optogenetic activation have recently been reported to provide optimized sets of photostimulation parameters and physiological conditions in the brain, retina, and human heart [20–28]. Computational models for quantitative analysis of the mechanism behind synaptic plasticity have also been reported and are continuously being improved based on recent experimental findings[29]. Such models provide mechanistic understanding of the dynamics of intracellular Ca^{2+} concentration, and the processes for long-term potentiation and long-term depression during different stimulation conditions[29,30]. New computational models that integrate the synaptic plasticity mechanism and optogenetic-mediated changes in specific ionic-concentration are required to theoretically study how expression of Ca^{2+}-permeable channels would affect the synaptic transmission and therefore plasticity under optical activation.

To ensure high prediction accuracy, the model must incorporate the stochastic nature of calcium dynamics in the postsynaptic spine. These dynamics arise from the random opening of N-methyl-D-aspartate (NMDA) receptors and voltage-dependent Ca^{2+} channels (VDCCs) in the postsynaptic spine[29]. Additionally, the model should account for variability in CapChR2 expression. Such a comprehensive approach can guide experimentalists in optimizing light stimulation parameters for current optogenetic variants, enabling the achievement of sufficient Ca^{2+} concentrations in the postsynaptic spine.

Hence, the objective of this paper is to study the optogenetic control of Ca^{2+}-based synaptic plasticity through subcellular expression of CapChR2 at the postsynaptic spine by formulating an integrated computational model that includes the stochastic effect. Further, to carry out a detailed analysis of the effect of amplitude and timing of three different combination of stimulations, namely, the presynaptic event, the postsynaptic event, and optogenetic activation of CapChR2 molecules at the postsynaptic spine, on the synaptic efficacy.

Results

To theoretically study the optogenetic control of synaptic plasticity, CapChR2 has been considered to be externally expressed at the postsynaptic spine, which allows Ca^{2+} ions to flow across the neuron membrane in response to light (Fig. 1a, b). The process of opening of CapChR2 channel, the flow of Ca^{2+}, and change in synaptic efficacy due to the activation of CapChR2 in the absence as well as in the presence of presynaptic and postsynaptic events have been studied in detail. The formulated computational model of the CapChR2 photocurrent is validated by comparing the simulated results with recently reported experimental results of Lahore et al. 2022 which are in good agreement [9] (Supplementary Fig. S1 and S2). For simulating the change in synaptic plasticity, the photocurrent model of CapChR2 has been integrated with a theoretical model of the evolution of synaptic plasticity state variables[29] (Fig. 1b). These state variables include the postsynaptic intracellular Ca^{2+} concentration $[Ca^{2+}]_i$, a leaky Ca^{2+} integrator (C^*) and synaptic efficacy (ρ). The theoretical model of Ca^{2+} concentration dynamics in response to presynaptic and postsynaptic events, occurring at different time lags has also been validated by comparing with reported results of Graupner et al. 2007 which are in good agreement (Supplementary Fig. S3)[29]. Although the formulated model is reductive, it effectively captures the key dynamics of calcium concentration changes and synaptic efficacy for the simplest synapse. The model is also well-suited to reproduce experimental findings, showing its validity and usefulness in understanding fundamental synaptic processes[9,29]. Changes in the above state variables have been studied in detail during the electrical stimulation

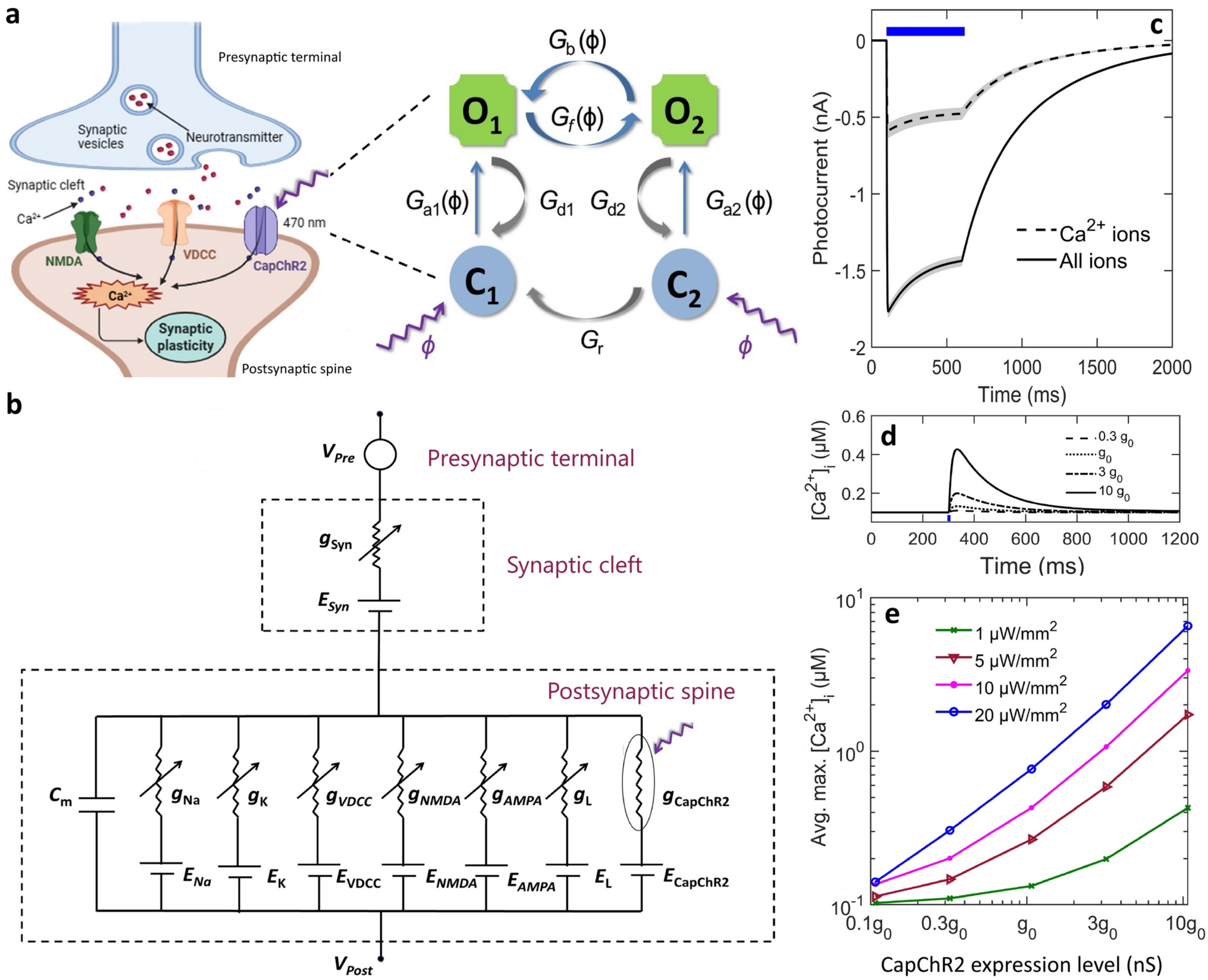

Fig. 1. Schematic and equivalent circuit diagram of optogenetic control of synaptic plasticity with calcium-permeable channelrhodopsin (CapChR2) expressed at the postsynaptic spine (**a**) Schematic of the process of synaptic transmission. Presynaptic neuronal firing releases neurotransmitters from synaptic vesicles. The Ca^{2+} concentration at the postsynaptic spine is increased by neurotransmitter-induced-triggering of natural Ca^{2+} conducting NMDA receptors, the voltage-dependent Ca^{2+} channel (VDCC), and externally expressed CapChR2. The photocurrent through CapChR2 channel is governed by the shown 4-state photocurrent model given on the right (for details see Methods). (**b**) Equivalent biophysical circuit diagram of above schematic, including currents through different natural ion channels and externally expressed CapChR2 across the neuron membrane. (**c**) Variation of the photocurrent with time in CapChR2 expressed in the neuron membrane at holding potential of -70 mV due to all ions and only Ca^{2+} ions on illumination with blue (470 nm) light for 500 ms at 10^3 µW/mm^2. (**d**) Variation of intracellular Ca^{2+} concentration $[Ca^{2+}]_i$, in the CapChR2 expressed postsynaptic spine with time on illumination with 1 µW/mm^2 for 10 ms at indicated CapChR2 expression level (g_0= 10.73 nS) (**e**) and corresponding variation of average of maximum $[Ca^{2+}]_i$ with CapChR2-expression density at different irradiances. The black lines represent the mean value and grey shaded envelop represents the standard deviation.

(I_{stim} = 3 nA, V_m = -70 mV) of the presynaptic terminal and the postsynaptic spine (I_{stim} = 3 nA, V_m = -70 mV), and the optogenetic activation of CapChR2-expressing postsynaptic spine.

In response to light, CapChR2 allows different ions, mainly Ca^{2+}, to flow across the membrane. The variation of photocurrent with time in CapChR2 due to all types of ions and only Ca^{2+} ions have been shown in Fig. 1c. CapChR2 contributes significantly higher Ca^{2+} based current, which is 2/3 of the total photocurrent. The maximum photocurrent is 1.7 ± 0.1 nA due to all ions and 0.58 ± 0.05 nA due to only Ca^{2+} ions (Fig. 1c). On illumination, the variation of $[Ca^{2+}]_i$ with time at different CapChR2-expression densities at the postsynaptic spine is shown in Fig. 1d. The results show that the activation of CapChR2 at 1 µW/mm^2 increases $[Ca^{2+}]_i$ from the steady-state concentration of 0.132 ± 0.001 µM to 0.43 ± 0.003 µM on increasing opsin expression level up to $10g_0$ (Fig. 1d). The maximum change in $[Ca^{2+}]_i$ with opsin expression density at different irradiances is shown in Fig. 1e. As is evident, the Ca^{2+} concentration can be controlled with both irradiance and expression level. At normal expression density, the average of maximum $[Ca^{2+}]_i$ achieves higher values up to 0.765 ± 0.006 μM at 20 μW/mm^2 (Fig. 1e).

CapChR2 photocurrent kinetics

The detailed photocurrent kinetics in CapChR2 at different photostimulation conditions are shown in Fig. 2. On illumination with short (10 ms) and long (500 ms) light pulses at 10^3 μW/mm^2, the CapChR2 photocurrent is 0.88 ± 0.02 nA and 1.74 ± 0.05 nA (Fig. 2a). The variation of normalized population density in different states with time is shown in Fig. 2b. Absorption of light at 470 nm triggers the CapChR2 photocycle. The molecules

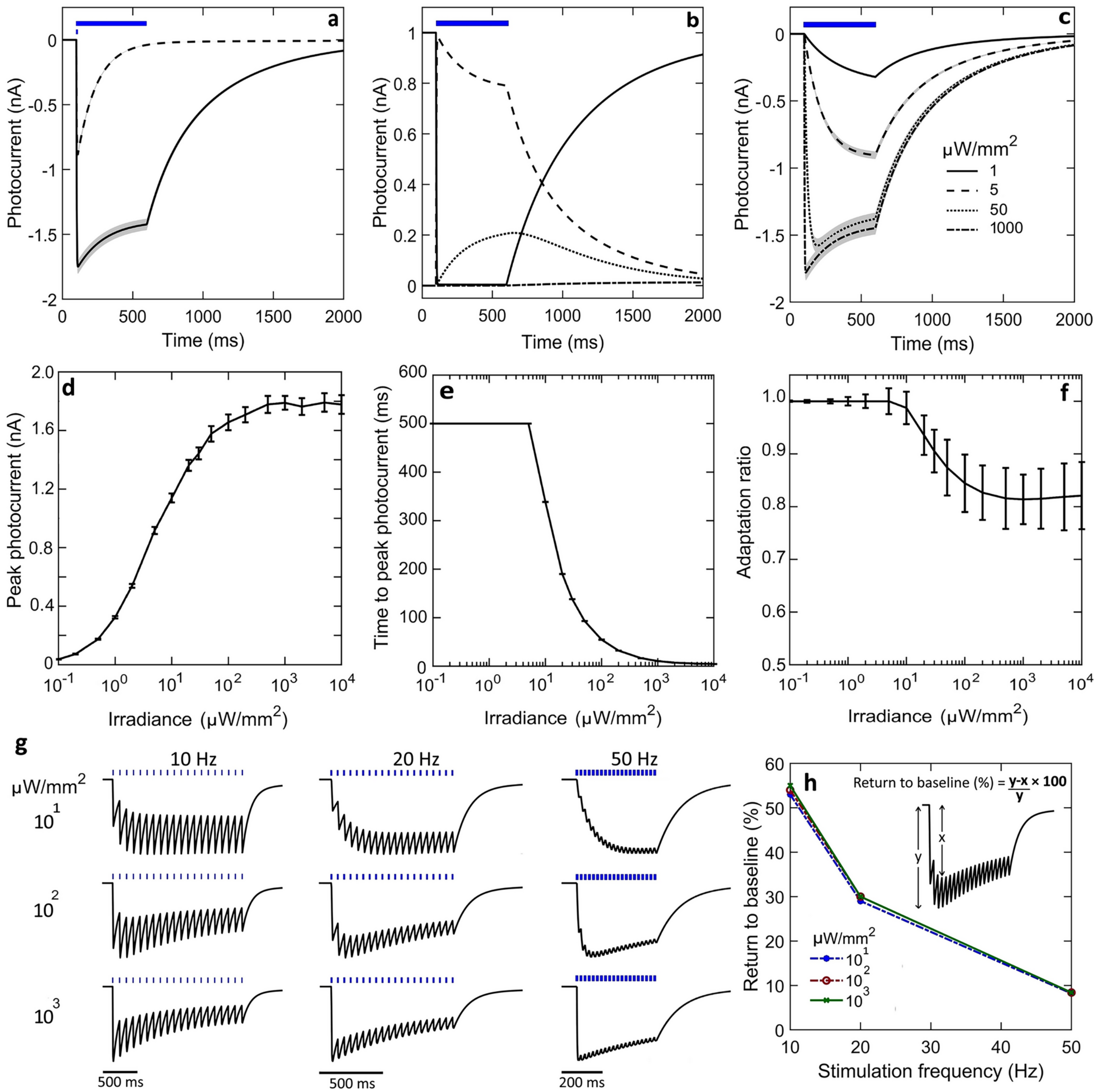

Fig. 2. CapChR2 photocurrent kinetics in CapChR2 on illumination with 470 nm light. (**a**) Variation of photocurrent with time on illumination at short (10 ms) and long (500 ms) light pulse at 10^3 μW/mm^2, and (**b**) corresponding variation of normalized population density of CapChR2 in different states with time for 10 ms light pulse. (**c**) Variation of photocurrent with time on illumination with 500 ms light pulse at indicated irradiances. (**d**–**f**) Effect of irradiance on (**d**) peak photocurrent, (**e**) time to peak photocurrent (t_{peak}), and (**f**) adaptation ratio with 500 ms light pulse. (**g**) Variation of photocurrent with time under multiple pulses at the indicated irradiances, and stimulation frequencies at a light pulse of 10 ms and (**h**) corresponding variation of return to baseline percentage with stimulation frequency. The black lines represent the mean value and grey shaded envelop represents the standard deviation.

switch from the closed state C_1 to the first open state O_1, which subsequently decays to second open state O_2, which is more stable due to its longer lifetime but is less conducting. On reaching O_1 and O_2, the CapChR2 channel opens rapidly to allow the flow of monovalent and divalent cations, especially Ca^{2+}. As turn-on kinetics of CapChR2 is flux-dependent, the population of the O_1 state becomes maximum during the light pulse. After light-off, the molecules relax to C_2 state for a longer period as it has the longest lifetime before returning to the ground state C_1.

The variation of photocurrent with time on illumination with a 500 ms light pulse at indicated irradiances is shown in Fig. 2c. It is evident from the variation that change in irradiance not only enhances the photocurrent amplitude but also speeds up the turn-on kinetics (Fig. 2c). The effect of irradiance on the photocurrent amplitude and kinetics in CapChR2 on illumination with a 500 ms light pulse is shown in Fig. 2d–f. The maximum photocurrent in CapChR2, saturates at 10^3 μW/mm^2 achieving a maximum value of 1.78 ± 0.04 nA (Fig. 2d). Faster photocurrent turn-on up to 4.55 ± 0.06 ms, in CapChR2, can be achieved at 10^4 μW/mm^2 (Fig. 2e). The adaptation ratio defined as the ratio of the plateau and to the peak photocurrent, is a key factor in determining the sustainability of spikes and the latencies of later spikes during the optogenetic activation of neurons. The adaptation ratio decreases with increasing irradiances as higher irradiances cause faster desensitization of the photocurrent. In CapChR2, adaptation ratio reaches 0.82 ± 0.06 at an irradiance of 10^4 μW/mm^2 in CapChR2 (Fig. 2f).

The photocurrent under multiple pulse stimulations and at varying frequencies is compared in Fig. 2 (g, h). Since the opsin molecules are unable to complete their photocycle before the arrival of subsequent light pulses, the photocurrent does not reach the baseline, resulting in a non-zero photocurrent plateau (Fig. 2g). The photocurrent plateau increases with increasing stimulation frequency. The results show that opsins with slow photocurrent turn-off kinetics exhibit a larger plateau. The percentage of return to baseline (RTB%) is a crucial factor to predict temporal resolution in optogenetic control. The formula to calculate RTB% is shown in inset of Fig. 2(h)[25]. The RTB% decreases with increasing stimulation frequency at different irradiances as shown in Fig. 2(h)[31].

Coincident electrical stimulation of presynaptic terminal and postsynaptic spine, and optogenetic activation of CapChR2-expressing postsynaptic spine

The variation of $[Ca^{2+}]_i$, C^* and ρ with time in response to electrical stimulation (I_{stim} = 3 nA, $V_{m,rest}$ = -70 mV) of presynaptic terminal, postsynaptic terminal and optogenetic activation of only the postsynaptic spine, and their coincident stimulation (I_{stim} = 3 nA, $V_{m,rest}$ = -70 mV, 470 nm, 1 ms) is shown in Fig. 3. During the optogenetic activation of the postsynaptic spine with a 1 ms light pulse at 470 nm, the variation of state variables with time is shown in Fig. 3a. It is evident that the change in $[Ca^{2+}]_i$ is irradiance dependent. At higher irradiances, C^* crosses the thresholds θ_d and θ_p and changes synaptic efficacy. Coincident electrical stimulation of presynaptic terminal (I_{stim} = 3 nA, $V_{m,rest}$ = -70 mV) and optogenetic activation at the postsynaptic spine is used to change the synaptic efficacy at reduced light irradiance (Fig. 3b). The time lag (Δt) between both the stimulation is zero. Similarly, coincident electrical stimulation of postsynaptic spine (I_{stim} = 3 nA, $V_{m,rest}$ = -70 mV) and optogenetic activation at the postsynaptic spine with zero time lag (Δt = 0) is also used to change the synaptic efficacy (Fig. 3c). Furthermore, the variation of $[Ca^{2+}]_i$, C^*, and ρ with time on coincident electrical stimulation (I_{stim} = 3 nA, $V_{m,rest}$ = -70 mV) of presynaptic terminal and postsynaptic spine and optogenetic activation (470 nm, 1 ms) at postsynaptic spine with Δt = 0 is shown in Fig. 3d.

The irradiance threshold to change synaptic efficacy reduces from 30 μW/mm^2 to 23.9 μW/mm^2 for coincident electrical stimulation of presynaptic terminal and optogenetic activation of postsynaptic spine, from 30 μW/mm^2 to 25 μW/mm^2, for coincident electrical stimulation and optogenetic activation of postsynaptic spine, and from 30 μW/mm^2 to 20 μW/mm^2 for coincident electrical stimulation of presynaptic terminal and postsynaptic spine, along with optogenetic activation of postsynaptic spine (I_{stim} = 3 nA, $V_{m,rest}$ = -70 mV, 470 nm, 1 ms) (Fig. 3(e–g)).

Effect of time lag (Δt) between optogenetic and electrical stimulations on synaptic efficacy

The synaptic efficacy is also affected by Δt between different combination of stimulations. The variation of $[Ca^{2+}]_i$, C^* and ρ with time during electrical stimulation of presynaptic terminal and optogenetic activation of CapChR2-expressing postsynaptic spine at different Δt is shown in Fig. 4(a) (upper), considering the presynaptic neuronal event to occur at t_0, and light pulse applied at t_0 + Δt. Negative values of Δt indicate that the light pulse is applied before the presynaptic neuronal event.

It is evident that Δt significantly alters the dynamics and amplitude of $[Ca^{2+}]_i$, and C^*, which are sufficient to change the synaptic efficacy. The corresponding average of maximum changes in amplitude of these variables with Δt is shown in Fig. 4a (lower). The study reveals the optimal Δt between electrical stimulation of presynaptic terminal and optogenetic activation of postsynaptic spine for achieving the change in the synaptic efficacy (I_{stim} = 3 nA, $V_{m,rest}$ = -70 mV, 470 nm, 1 ms). From Fig. 4a (lower) the maximum change in synaptic efficacy occurs at Δt = -100 ms. At 23 μW/mm^2, the maximum change in synaptic efficacy is 0.19 ± 0.05 for Δt = -100 ms.

Considering the postsynaptic neuronal event to occur at t_0, and light pulse applied at t_0 + Δt, the maximum change in synaptic efficacy occur at Δt = –200 ms (Fig. 4b). At 25 μW/mm^2, the maximum change in synaptic efficacy is 0.18 ± 0.07 for Δt = –200 ms (Fig. 4b, lower). Considering presynaptic neuronal event to occur at t_{pre} and postsynaptic neuronal event at $t_{post} = t_{pre}$ + Δt, the average of maximum amplitude of $[Ca^{2+}]_i$ is 2.44 ± 0.54 μM at 10 ms time lag (Supplementary Fig. 4). However, the corresponding change in C^* is not able to cross the thresholds θ_d or θ_p. For optimizing the light irradiance during electrical stimulation (I_{stim} = 3 nA, $V_{m,rest}$ = -70 mV) and optogenetic activation (470 nm, 1 ms), the electrical stimulations to presynaptic terminal and postsynaptic spine are applied at t_0 and t_0 + 10 ms, respectively. Light pulse is applied at t_0 + Δt (Fig. 4c,

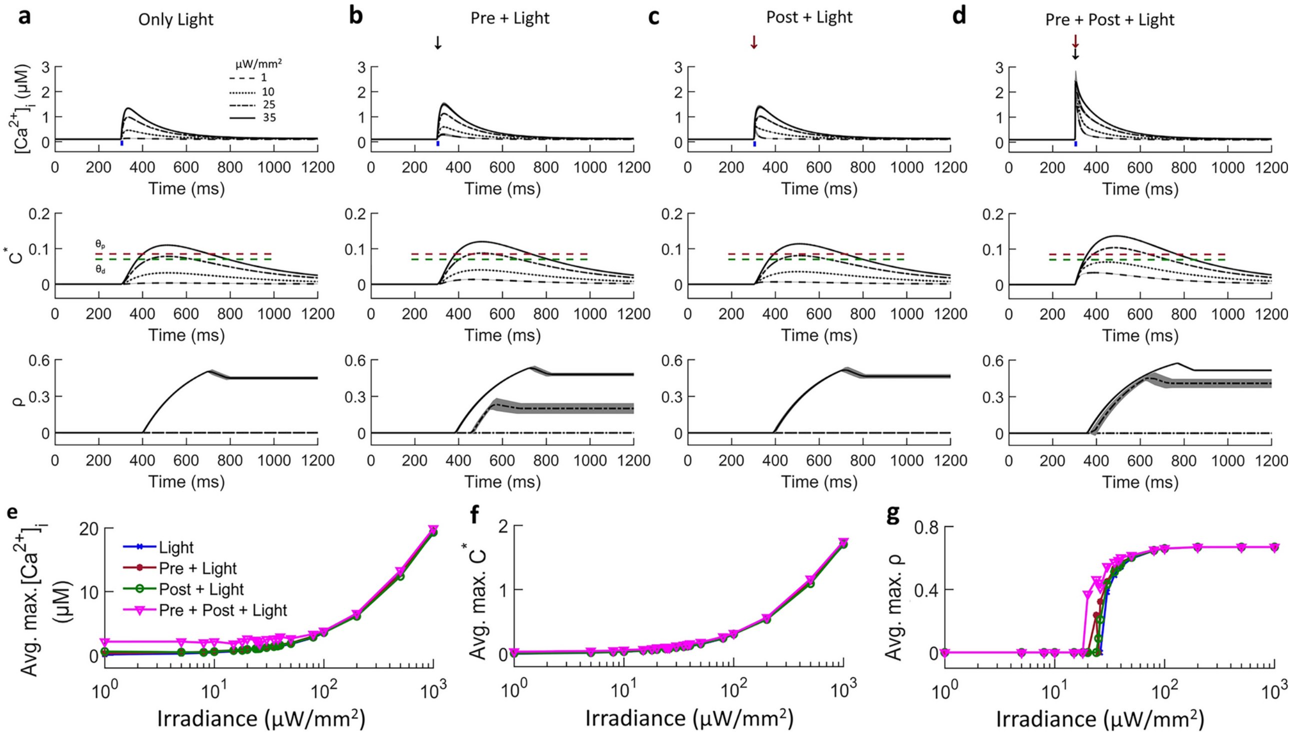

Fig. 3. Evolution of the state variables of the synaptic plasticity model (postsynaptic intracellular calcium concentration ($[Ca^{2+}]_i$), leaky calcium integrator (C^*), synaptic efficacy (ρ)) during different pairs of electrical stimulation of presynaptic terminal and postsynaptic spine, and optogenetic activation of the CapChR2-expressing postsynaptic spine. (**a**–**d**) Variation of $[Ca^{2+}]_i$, C^*, and ρ with time (**a**) On optogenetic (470 nm, 1 ms) activation of postsynaptic spine at indicated irradiances. (**b**) Coincident optogenetic activation of the postsynaptic spine with electrical stimulation of only presynaptic terminal (I_{stim} = 3 nA, $V_{m,rest}$ = -70 mV, 470 nm, 1 ms). (**c**) Coincident optogenetic activation of the post synaptic spine with electrical stimulation of only the postsynaptic spine (I_{stim} = 3 nA, $V_{m,rest}$ = -70 mV, 470 nm, 1 ms). (**d**) Coincident optogenetic activation of the postsynaptic spine with electrical stimulation of both the presynaptic terminal and the postsynaptic spine with no time lag (Δt) (I_{stim} = 3 nA, $V_{m,rest}$ = -70 mV, 470 nm, 1 ms). θ_d and θ_p denotes the thresholds for depression and potentiation, respectively. The black lines represent the mean value and grey shaded envelop represents the standard deviation. (**e**–**g**) Corresponding variation of average of maximum achievable values of (**e**) $[Ca^{2+}]_i$, (f) C^*, and (g) ρ with irradiance in different stimulation conditions.

Upper). At 18 μW/mm², the maximum change in the synaptic efficacy is 0.39 ± 0.4 at Δt = –100 ms (Fig. 4c, lower).

Effect of frequency of optogenetic and electrical stimulations on synaptic efficacy

The effect of stimulation frequency of electrical stimulation of presynaptic terminal and postsynaptic spine, and optogenetic activation of CapChR2-expressed postsynaptic spine is shown in Fig. 5(a-c). The variation of $[Ca^{2+}]_i$, and C^* with time at different frequencies have been shown in Fig. 5. The corresponding variation of synaptic efficacy with stimulation frequency for different kinds of stimulations are shown in Fig. 5d–f. At a low frequency (5 Hz) stimulation, the minimal Ca^{2+} influx leads to insufficient increase in C^*, preventing it from crossing the thresholds θ_d and θ_p. Presynaptic terminal and postsynaptic spine alone are not able to trigger synaptic plasticity at any stimulation frequency (Fig. 5(d, e)). In contrast to the above electrical stimulations, optogenetic activation (470 nm, 1 ms) of CapChR2-expressing postsynaptic spine changes synaptic efficacy above 5 Hz at 8 μW/mm² (Fig. 5f). The frequency threshold for optogenetic activation (470 nm, 1 ms) is irradiance dependent. On increasing light irradiance, the synaptic efficacy can be changed at lower frequencies (Fig. 5f).

Discussion

The present study proposes a novel method of direct optogenetic control of intracellular Ca^{2+} concentration at postsynaptic spine-genetically expressed with CapChR2. A detailed theoretical analysis shows that optogenetic activation of postsynaptic spine results in a larger increase in postsynaptic intracellular Ca^{2+} level than individual or coincident presynaptic or postsynaptic events. Hence, optogenetic control leads to effective change in synaptic efficacy at very low irradiances. Minimum irradiance threshold required for changing synaptic efficacy in the presence and absence of presynaptic and postsynaptic events has been determined. The theoretical study also helped in finding the optimal range of time lags among different combination of stimulations to efficiently change synaptic efficacy.

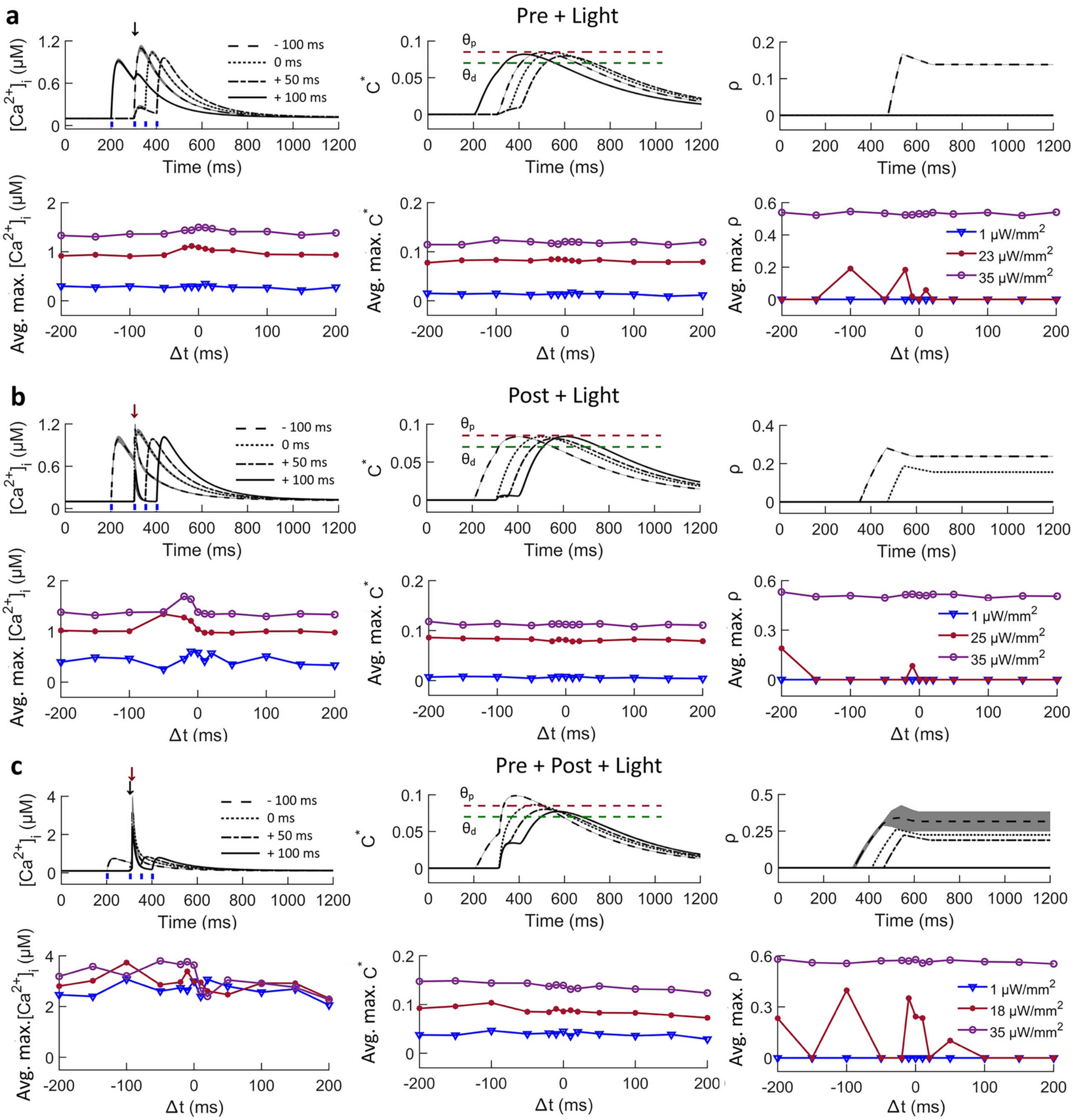

Fig. 4. Effect of time lag (Δt) on optogenetic activation of CapChR2-expressing postsynaptic spine, electrical stimulation of presynaptic terminal, and postsynaptic spine on the plasticity model state variables (calcium concentration $[Ca^{2+}]_i$, leaky calcium integrator (C^*), synaptic efficacy (ρ). (**a**–**c**) Variation of (upper) state variables with time on applying different stimulus at different time lags (Δt) and (lower) maximum of state variables with time lag between different stimulus at indicated light irradiances during (a) light with presynaptic event (I_{stim} = 3 nA, $V_{m,rest}$ = -70 mV, 470 nm, 1 ms), (b) light with postsynaptic event (I_{stim} = 3 nA, $V_{m,rest}$ = -70 mV, 470 nm, 1 ms), and (c) light with both presynaptic and postsynaptic events (I_{stim} = 3 nA, $V_{m,rest}$ = -70 mV, 470 nm, 1 ms). The light irradiance is 23 μW/mm² for (**a**) and 25 μW/mm² for (b). For (**c**), the time lag between presynaptic and postsynaptic event is 10 ms and light irradiance is 18 μW/mm². The timing of light (t_{light}), postsynaptic event (t_{post}), and presynaptic event (t_{pre}) are such that $t_{light} = t_{pre}$ + Δt or $t_{light} = t_{post}$ + Δt. θ_d and θ_p are the thresholds for depression and potentiation, respectively. The black lines represent the mean value and grey shaded envelop represents the standard deviation.

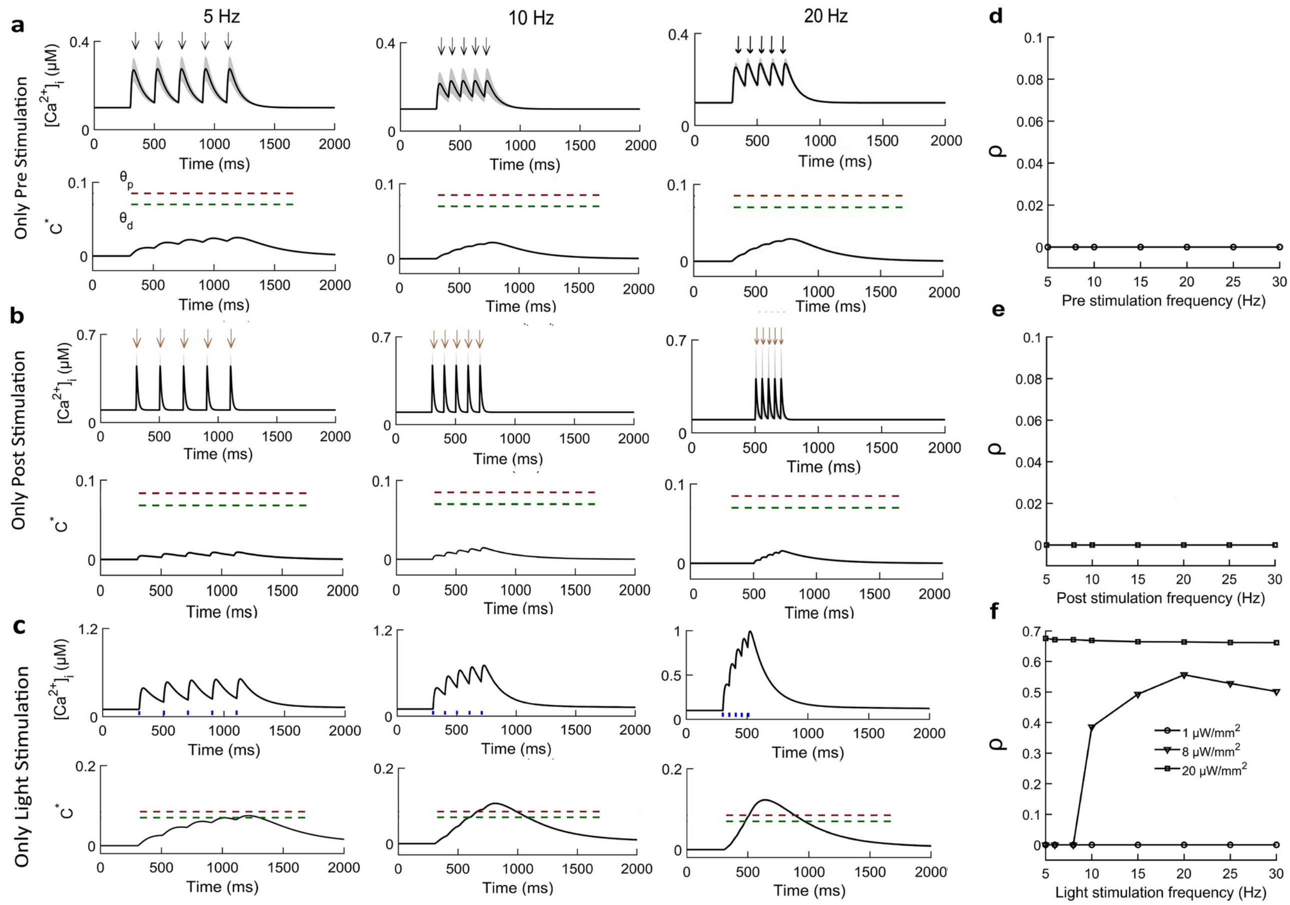

Fig. 5. Effect of stimulation frequency of electrical stimulation of only presynaptic terminal and only postsynaptic spine, and optogenetic activation of only postsynaptic spine on the synaptic efficacy. (**a**–**c**) Variation of postsynaptic calcium concentration $[Ca^{2+}]_i$ and leaky calcium integrator (C^*) with time on repetitive electrical stimulation (I_{stim} = 3 nA, $V_{m,rest}$ = -70 mV) of (a) only presynaptic event, (b) only postsynaptic event, and (c) only postsynaptic spine stimulation with light (470 nm, 1 ms light pulse) at 8 μW/mm^2, at indicated frequencies. (**d**–**f**) Corresponding variation of synaptic efficacy with stimulation frequency at (d) only presynaptic stimulation, (**e**) only postsyanptic stimulation, and (**f**) only optogenetic activation of postsynaptic spine at indicated irradiances. θ_d and θ_p are the threshold for depression and potentiation. The black lines represent the mean value and grey shaded envelop represents the standard deviation.

Prior studies have shown that light-evoked action potentials using ChR2 in neurons lead to enhanced Ca^{2+} concentration which thereby changes the probability of neurotransmitter release[15]. The mechanism behind the Ca^{2+} increase in the above experiment is due to increased activation of voltage-gated Ca^{2+} channels in the targeted neuron, which indirectly increases the intracellular Ca^{2+} level. Recent studies have shown that type 1 viral ChRs accumulate exclusively intracellularly, and upon illumination, induce Ca^{2+} release from intracellular IP3-dependent stores that is proportional to the applied light irradiance[32]. The present method of direct optogenetic control of Ca^{2+} concentration through CapChR2 would be a potential alternative to the above methods developed for controlling synaptic plasticity.

Synaptic efficacy depends on many factors that include the presynaptic transmitter release machinery, postsynaptic receptors and signal transduction pathways, gene activation and synthesis of new proteins[33,34]. Experimental data and computational models indicate that the precise timing and the temporal order of pre and postsynaptic events can drive changes in synaptic strength, collectively called spike-timing dependent plasticity[35–37]**.** In the present study, it is explicitly shown that coincident stimulation of presynaptic and postsynaptic event helps in minimizing the irradiance thresholds for optogenetic activation to change synaptic efficacy. The light irradiance threshold reduces from 30 μW/mm^2 to 23.9 μW/mm^2 on coincident optogenetic activation of postsynaptic spine with electrical stimulation of presynaptic event (I_{stim} = 3 nA, $V_{m,rest}$ = -70 mV, 470 nm, 1 ms) (Fig. 3g). The irradiance can be further reduced up to 20 μW/mm^2 on coincident electrical stimulation of presynaptic terminal, postsynaptic spine and optogenetic activation of postsynaptic spine (I_{stim} = 3 nA, $V_{m,rest}$ = -70 mV, 470 nm, 1 ms) (Fig. 3g). Earlier experimental and theoretical studies have shown that the precise timing of stimulation can influence the direction of synaptic plasticity[37]. The present analysis shows that the change in synaptic efficacy can be maximized by optimizing the time lag between different combinations of stimulation. The optimal time lag is + 10 ms for postsynaptic event relative to presynaptic event (I_{stim} = 3 nA, $V_{m,rest}$ = -70 mV) (Supplementary Fig. S4).

Mimicking natural patterns of neuronal activity may induce more physiologically relevant changes in synaptic strength[38]. Recently, a comprehensive study on the effect of temporal shaping of light pulses on optogenetically evoked firing patterns has shown that non-square temporal shapes of light pulses help in generating naturalistic firing patterns with different types of ChRs[38]. The present method of optogenetic control of Ca^{2+} dynamics opens opportunities to study the effect of more naturalistic stimulations by pulse shaping. Under multiple pulses, stimulation frequencies determine the integrated Ca^{2+} concentration that can influence the magnitude of synaptic plasticity[37,39]. The study explicitly shows that repetitive firing of a presynaptic event does not alter synaptic efficacy (Fig. 5a). For optogenetic activation, the slow turn-off kinetics of CapChR2 results in a sustained increase in Ca^{2+} ions even after the light is switched off. Hence, under multiple pulses, the optogenetic control does not show any upper limit for the stimulation frequency (Fig. 5).

In optogenetics, the total photocurrent through opsin-channels is directly proportional to their expression density, affecting the irradiance thresholds for any action. Notably, the recently discovered CapChR2 inherently exhibits a substantial photocurrent, providing robust excitation even at normal expression densities. However, attempting a functional-level response by increasing the expression of the optogenetic sensor protein poses challenges due to the elevated risk of cell toxicity and immune response[40]. The scaling factor for the contribution of Ca^{2+} through activation of CapChR2 molecules at the presynaptic terminal ($\beta_{CapChR2}$) accounts for any changes in the opsin-expression level. In the present study, there is a significant change in the Ca^{2+} concentration even at a very small value of $\beta_{CapChR2}$ (~ 10^{-6}), which is three orders of magnitude lower than the scaling factors used for NMDA receptor and VDCC channel (Supplementary Fig. S5).

The spine neck resistance plays a key role in regulating electrical signal propagation between the spine head and dendrite, influencing the depolarization of the spine compartment and the interaction between pre- and postsynaptic elements[41]. It can vary based on factors such as, spine morphology and location within the neuron. Studies have shown that the pairing of pre- and postsynaptic activity is highly dependent on spine neck resistance[42]. High resistance isolates the spine head, increasing localized depolarization while diminishing its impact on the dendrite. Low resistance, on the other hand, allows depolarization to spread more efficiently to the dendrite, enhancing overall neuron excitability. An average spine neck resistance of around 500 MΩ has been shown to influence both depolarization and spine-dendrite coupling, affecting synaptic strength and Ca^{2+} signaling[43].

In the brain microcircuits, each neuron receives thousands of synaptic inputs distributed across an extensive dendritic tree[44]. The localized opsin-expression would allow for fine-tuned modulation of synaptic efficacy in response to various stimuli or activity patterns, offering prospects for unraveling the intricacies of neural circuit function and information processing. However, the compartment-specific opsin-expression is challenging[45]. In optogenetics, multi-photon excitation techniques are used to get 3-dimensional (3D) spatially precise control of opsin molecules in the tissue volume[46–48]. These advanced light illumination methods use longer wavelengths, allowing deeper excitation with minimal attenuation. The 3D resolution of such methods would further enhance the spatial resolution for targeting the presynaptic terminal. However, the response of CapChR2 under two-photon excitation is yet to be analyzed.

CapChR2 requires blue light which faces strong absorption and scattering in the biological tissue. This would remain a challenge for testing this method in in vivo study. However, intense research efforts are being made to design efficient light delivery methods for in vivo optogenetics that include, two-photon excitation, use of upconversion nanoparticles to locally convert NIR to visible and to get red-shifted excitation spectrum through mutations[49–51]. Integration of these technologies would help in optogenetic control of synaptic plasticity using the proposed method.

The present work provides the first approach of direct optogenetic control of Ca^{2+}-based synaptic plasticity. The fast opsin kinetics allow temporally precise control of Ca^{2+} concentration. Moreover, the irradiance-dependent change in the amplitude of Ca^{2+} concentration and synaptic efficacy is also an additional advantage of this method. This study is important for understanding synaptic plasticity, memory formation, and Ca^{2+} -dependent signaling pathways in neurons.

Methods

The Ca^{2+} ions influx into the neuron through various kinds of ion-channels. At the postsynaptic spine, the NMDA receptor and VDCC play major roles in maintaining the intracellular Ca^{2+} concentration[29,52]. The dynamics of Ca^{2+} through these channels in response to presynaptic and postsynaptic stimulations can be effectively modelled using the earlier reported theoretical models[29]. In this study, CapChR2 is considered to be genetically expressed at the postsynaptic spine. Therefore, the light-induced flow of Ca^{2+} ions through these channels would also contribute to the dynamics of intracellular Ca^{2+} at the postsynaptic spine.

Dynamics of CapChR2-mediated current

Optogenetics involves light-sensitive microbial proteins as light-gated ion-channels, enabling the optical modulation of neuron membrane potential[53,54]. These proteins detect light through embedded retinal chromophores within their structure[55]. On illumination, the retinal chromophore undergoes ultrafast (~ fs) photoisomerization, initiating the protein photocycle with different intermediate states[56–59]. Some of these intermediate states are involved in forming a pore across the membrane to allow ions to flow, resulting in an ionic current.

The rate of ion flow depends on several factors that include instantaneous opsin molecule population density in the open-states, unitary conductance and expression density of the opsin channels, concentration gradient of permeable ions across the membrane, and membrane potential [25,60,61]. Therefore, the current through the CapChR2 molecules embedded within the neuron membrane can be expressed as,

$$I_{CapChR2} = g_o f_\phi\left(\phi, t\right) G\left(V\right) f_m(\left[Ca^{2+}\right]_o) \tag{1}$$

where g_o is total conductance, accounting for both unitary conductance and CapChR2 expression density. $G\left(V\right)$ is the voltage-dependent rectification function is defined as $G\left(V\right) = \left(A + B\exp\left(-\left(V_m - E_{CapChR2}\right)/C\right)\right)$, where A, B and C are the constants. V_m is the postsynaptic neuron membrane potential and $f_m(\left[Ca^{2+}\right]_o)$ is the outer Ca^{2+} ion concentration $[Ca^{2+}]_o$-dependent function[23,27]. $f_\phi\left(\phi, t\right)$ is a normalized light-dependent function. It accounts for the population density of opsin molecules in the open state, which depends on the effective photon flux density (ϕ), and the kinetics of the photocycle intermediates[61]. ϕ depends on wavelength (λ), and light irradiance (I). It is the photon flux per unit area per unit time, defined as $\lambda I/hc$, where h is Planck's constant and c is the speed of light in vacuum[61]. $E_{CapChR2}$ is the reversal potential for CapChR2 channel that depends on intra- and extra-cellular Ca^{2+} concentrations[9].

In general, the photocycle of ChRs involves a few open conducting and several non-conducting intermediate states, besides the ground state[55]. For determining the population density of the molecule in the open states, a four-state photocycle model for CapChR2 has been considered based on earlier reported models[25,61]. The four-state photocycle model consists of two-closed ground (C_1 and C_2) and two-open conducting (O_1 and O_2) states. In dark, opsin molecule rests in ground state C_1, which switches from state C_1 to O_1 on illumination. From the first conducting state O_1, molecules either switch to second conducting state O_2 or decay back to ground state C_1. Conducting state O_2 is less conductive but has a longer lifetime than O_1. From state O_2, it either switches to state O_1 or decays to state C_1. The reversible transition takes place between state O_1 and O_2, which can be both thermally relaxed and light-induced. From C_2, it can either be photo-excited back to O_2 or can thermally relax to C_1. The switching rate of molecules from C_2 to C_1 is much slower than other rate constants[24,26].

Considering, C_1, O_1, C_2, and O_2 to denote the instantaneous fraction of CapChR2 molecules in each of the four states such that $C_1 + O_1 + O_2 + C_2 = 1$, the change of populations with time can be described as,

$$\dot{C}_1 = G_{d1}O_1 - G_{a1}\left(\phi\right)C_1 + G_rC_2 \tag{2}$$

$$\dot{O}_1 = G_{a1}(\phi)\,C_1 - \left(G_{d1} + G_f\left(\phi\right)\right)O_1 + G_b(\phi)\,O_2 \tag{3}$$

$$\dot{O}_2 = G_{a2}(\phi)\,C_2 - \left(G_{d2} + G_b\left(\phi\right)\right)O_2 + G_f\left(\phi\right)O_1 \tag{4}$$

$$\dot{C}_2 = G_{a2}(\phi)\,O_2 - \left(G_{a2}(\phi) + G_r\right)C_2 \tag{5}$$

where, $G_{a1}, G_{a2}, G_{d1}, G_{d2}, G_f, G_b$ and G_r are the rate constants for transitions $C_1 \to O_1, C_2 \to O_2, O_1 \to C_1, O_2 \to C_2, O_1 \to O_2, O_2 \to O_1$ and $C_2 \to C_1$ respectively. The light-dependent rate functions can be described as $G_{a1}\left(\phi\right) = k_1\phi^p/(\phi^p + \phi_m^p)$,$G_{a2}\left(\phi\right) = k_2\phi^p/(\phi^p + \phi_m^p)$, $G_f\left(\phi\right) = G_{f0} + k_f\phi^q/(\phi^q + \phi_m^q)$, and $G_b\left(\phi\right) = G_{b0} + k_b\phi^q/(\phi^q + \phi_m^q)$ [22]. Since there are two open states in the 4-state model, $f_\phi\left(\phi, t\right) = O_1 + \gamma O_2$, where γ = 0.05, the ratio of conductance of the open states. The model parameters for the photocurrent of CapChR2 have been taken from reported experimental results[9] (Table 1).

Experimental results with CapChR2 have been reported in hippocampal neurons[9]. The photocurrent amplitude has been matched to get total conductance value for the present model, which is 32.2 nS at $\left[Ca^{2+}\right]_o$ = 70 mM[9]. At postsynaptic spine, the intracellular Ca^{2+} concentration is 0.1 μM and the reversal potential is 2 mV. Therefore, the extracellular Ca^{2+} concentration determined using the Nernst's equation, $\left[Ca^{2+}\right]_o$ = 5 mM. Thus, the total conductance gets reduced to 16.1 nS. The total conductance is further reduced to 2/3 of 16.1, due to permeability ratio ($P_{Ca}/P_{Na} = 1.9$) [9]. Hence, the effective conductance at the postsynaptic spine is 10.73 nS.

To investigate the variability in the stochastic nature of the expression level of CapChR2, Gaussian noise with a mean of zero and a variance equal to 5% of the total CapChR2 conductance has been incorporated in the model.

Calcium dynamics at postsynaptic spine

The rate of change of $[Ca^{2+}]_i$ at postsynaptic spine can be expressed as,

$$\frac{d[Ca^{2+}]_i}{dt} = -\frac{\left([Ca^{2+}]_i - [Ca_0^{2+}]_i\right)}{\tau_{Ca}} - \xi(\beta_{NMDA}I_{NMDA} + \beta_{VDCC}I_{VDCC} + \beta_{CapChR2}I_{CapChR2}) \tag{6}$$

where τ_{Ca} is the single exponential time constant of the passive decay process, and $[Ca_0^{2+}]_i$ is the Ca^{2+} resting concentration[29]. I_{NMDA} and I_{VDCC} are the Ca^{2+} component of currents through the NMDA receptors and VDCC-channels, respectively. ξ converts ionic currents into concentration changes per unit time for a spine volume of 1 μm^3 [29]. $I_{CapChR2}$ is the light-dependent Ca^{2+} current through CapChR2 channels. β_{NMDA}, β_{VDCC}, and $\beta_{CapChR2}$ are the scaling factors for I_{NMDA}, I_{VDCC}, and $I_{CapChR2}$ currents, respectively[29].

Parameter	Values
G_{d1}	6.09×10^{-3} ms^{-1}
G_{d2}	9.09×10^{-5} ms^{-1}
G_{f0}	1.1×10^{-3} ms^{-1}
G_{b0}	5.0×10^{-4} ms^{-1}
G_r	9×10^{-5} ms^{-1}
k_1	2 ms^{-1}
k_2	0.18 ms^{-1}
k_f	1.1×10^{-4} ms^{-1}
k_b	1.4×10^{-3} ms^{-1}
p	1
q	1
ϕ_m	5.5×10^{15} photons mm^{-2} s^{-1}
g_o	32.2 nS
$\sigma_{CapChR2}$	5% of g_o
$\beta_{CapChR2}$	1×10^{-6}
$E_{CapChR2}$	2 mV
$f_m(\left[Ca^{2+}\right]_o)$	0.5 at $\left[Ca^{2+}\right]_o = 0.1\mu M$
λ	470 nm
A	28.7
B	-28
C	30.6

Table 1. Model parameters for opsin channel CapChR2[9].

Further, rate of change in the leaky Ca^{2+} integrator (C^*), used to capture the modulation of frequency response for long term changes in synaptic efficacy, while maintaining the simple threshold plasticity mechanism, is expressed as,

$$\frac{dC^*}{dt} = -\frac{C^*}{\tau_*} + ([Ca^{2+}]_i - [Ca_0^{2+}]_i) \tag{7}$$

where, τ_* is the integration time constant[30]. This mechanism integrates Ca^{2+} over longer time scales to drive plasticity, as could arise from the interplay of fast and a slow-buffers in the spine head[30].

The expression of synaptic plasticity takes the form of persistent changes to synaptic parameters, which we assume here to be driven by integrated calcium (C^*). To model these persistent changes, we consider a model of a single synapse subjected to trains of presynaptic and postsynaptic Aps[62]. The model represents the state of a synapse as a synaptic efficacy variable (ρ), whose temporal evolution is described by a first-order differential equation as,

$$\frac{d\rho}{dt} = (-\rho(1-\rho)(0.5-\rho) + \gamma_p(1-\rho)\Theta[C^* - \theta_p] - \gamma_d\rho\Theta[C^* - \theta_d]/\tau \tag{8}$$

where, τ is time constant of convergence of the synaptic efficacy, $\rho = 0.5$ is unstable fixed point separating the basins of attraction of the two stable states (depressed at $\rho = 0$ and potentiated at $\rho = 1$), Θ is Heaviside function, θ_d and θ_p are depression and potentiation thresholds, and γ_d and γ_p are depression and potentiation rates, respectively[30,62]. Previous computational studies suggest that changes in synaptic efficacy, characterized by transitions between UP (potentiated) and DOWN (depressed) states, are mediated by postsynaptic calcium concentration. High intracellular calcium concentrations trigger synaptic potentiation, whereas prolonged low calcium signals induce synaptic depression[63].

Noisy calcium transients

To incorporate the stochasticity in the model, two sources of noise have been considered. (i) the maximum conductance of NMDA receptors, randomly assigned at each presynaptic spike, and (ii) the maximum conductance of voltage-dependent Ca^{2+} channels, randomly assigned at each postsynaptic spike[29]. Both conductances are drawn from binomial distributions, defined by the total number of channels N_{total} and the opening probability per channel p_o. Each presynaptic or postsynaptic spike results in an integer number n_o of NMDA or VDCC channel openings, respectively. We assume the channels open independently[29]. The single-channel conductance g_{single} is chosen so that the mean Ca^{2+} amplitudes match the specified values[29]. To capture the stochastic nature of Ca^{2+} ion influx, Gaussian noise with zero mean and variance proportional to n_o is added to $n_o * g_{single}$ [29]. The parameters for the NMDA and VDCC maximum conductance distributions are adapted from Graupner et al. 2007[29].

Membrane potential dynamics at postsynaptic spine

The rate of change of membrane potential in postsynaptic spine depends on several nonlinear natural ionic currents and externally applied electric current (I_{Stim}) as,

$$C_m \frac{dV_m}{dt} = -(I_{Na} + I_K + I_{VDCC} + I_L + I_{NMDA} + I_{AMPA}) + I_{Stim} \tag{9}$$

where C_m is cell capacitance and I_{Stim} is input current to postsynaptic spine[29]. Leak current can be described as follows, $I_L = g_L (V_m - E_L)$, where g_L is the leak conductance and E_L is the reversal potential[29].

Gating mechanism of different ion-channels and receptors

Among the above ionic currents, I_{Na}, I_K, and I_{VDCC} can be described as, $I_{ionic} = g_{ionic} m^p h^q (V_m - E_{ionic})$, where g_{ionic} is maximal conductance, m is activation variable (with exponent p), h is inactivation variable (with exponent q), and E_{ionic} is reversal potential[29]. The kinetics of each of the gating functions x (m or h) depends on voltage-dependent gating functions of each ion channel (α_x and β_x) as described in Table 2, and obeys first-order kinetics as,

$$\dot{x} = (x_\infty - x) / \tau_x \tag{10}$$

Voltage dependent gating functions (x_∞ and τ_x) and values for parameters for postsynaptic spine model are given in Tables 2 and 3 respectively[29].

$$I_{AMPA} = g_{AMPA} s_{AMPA} (V_m - E_{AMPA}) \tag{11}$$

where g_{AMPA} is maximum AMPA current conductance, s_{AMPA} is a single exponentially decaying gating variable with a finite rise time and E_{AMPA} is AMPA-mediated current reversal potential. At each occurrence of presynaptic spike at time t_k, variable x_{AMPA} is increased by one, which can be modelled as,

$$\dot{s}_{AMPA} = -s_{AMPA}/\tau_{AMPA} + \alpha_S x_{AMPA} (1 - s_{AMPA}) \tag{12}$$

$$\dot{x}_{AMPA} = -x_{AMPA}/\tau\prime_{AMPA} + \alpha_x \sum \delta (t - t_k) \tag{13}$$

$$I_{NMDA} = g_{NMDA} s_{NMDA} B(V) (V_m - E_{NMDA}) \tag{14}$$

where g_{NMDA} is the maximum NMDA receptor-mediated current conductance and $B(V)$ is defined as the voltage dependence of magnesium block as,

$$B(V) = \frac{1}{1 + exp(-0.08V) \frac{[Mg^{2+}]}{0.69}} \tag{15}$$

where $[Mg^{2+}]$ is the extracellular magnesium concentration, which controls the voltage dependence[64,65]. The gating variable s_{NMDA} can be defined as,

$$\dot{s}_{NMDA} = -s_{NMDA}/\tau_{NMDA} + \alpha_S x_{NMDA} (1 - s_{NMDA}) \tag{16}$$

$$\dot{x}_{NMDA} = -x_{NMDA}/\tau'_{NMDA} + \alpha_x \sum \delta (t - t_k) \tag{17}$$

The optogenetic response of CapChR2-expressing postsynaptic spine on stimulation at different photostimulation conditions is studied through numerical simulations using Eqns. (1–17), with gating functions and parameters, given in Tables 1–3. All simulations have been carried out in MATLAB and the program code is publicly available in the Zenodo repository[66].

I_{ionic}	Gating variable	x_∞	τ_x
I_{Na}	$p = 3$ $q = 1$	$\frac{1}{\exp[-0.11(V_m+36)]+1}$ $\frac{1}{\exp[0.14(V_m+44.1)]+1}$	0.1 $\frac{3.5}{\exp[0.25(V_m+35)]+\exp[-0.04(V_m+35)]} + 1$
I_K	$p = 4$	$\frac{1}{\exp[-0.04(V_m+30)]+1}$	$\frac{2.5}{\exp[0.025(V_m+30)]+\exp[-0.02(V_m+30)]} + 1$
I_{VDCC}	$p = 3$	$\frac{1}{\exp[-(V_m+37)]+1}$	3.6
	$q = 1$	$\frac{1}{\exp[2(V_m+41)]+1}$	29

Table 2. Gating function parameters of sodium-, potassium-, and voltage-dependent calcium channels[29,30].

Parameter	Definition	Value
g_{Na}	Maximum I_{Na} current conductance	0.7 μS
g_K	Maximum I_K current conductance	1.3 μS
g_{VDCC}	Maximum I_{VDCC} current conductance	$5.6\times10^{-4}\mu S$
g_{NMDA}	Maximum I_{NMDA} current conductance	$4.5\times10^{-4}\mu S$
g_{AMPA}	Maximum I_{AMPA} current conductance	0.0195 μS
g_L	Maximum I_L current conductance	0.005 μS
$g_{CapChR2}$	Maximum $I_{CapChR2}$ current conductance	10.73 nS
E_{Na}	Sodium reversal potential	60 mV
E_K	Potassium reversal potential	-80 mV
E_L	Leak reversal potential	-68.03 mV
E_{VDCC}	VDCC-mediated current reversal potential	140 mV
E_{NMDA}	NMDA-mediated current reversal potential	0 mV in neuron, 140 mV in calcium dynamics
E_{AMPA}	AMPA-mediated current reversal potential	0 mV
τ_{AMPA}	Time constant	$2ms$
$\tau\prime_{AMPA}$	Time constant	$0.05ms$
α^S_{AMPA}	–	$1ms^{-1}$
α^x_{AMPA}	–	1
τ_{NMDA}	Time constant	$80ms$
$\tau\prime_{NMDA}$	Time constant	$2ms$
α^S_{NMDA}	–	$1ms^{-1}$
α^x_{NMDA}	–	1
I_{Stim}	Input electrical current to postsynaptic neurons	3 nA
$\left[Mg^{2+}\right]$	Extracellular magnesium concentration	$1mM$
C_m	Cell capacitance	0.1 nF
$[Ca_0^{2+}]_i$	Calcium resting concentration	$0.1\mu M$
ξ	Conversion factor (ionic currents into concentration changes per unit time)	$5.18\times10^4 m^2\mu M/C$
β_{NMDA}	Scaling factor for NMDA-mediated current	0.0278
β_{VDCC}	Scaling factor for VDCC-mediated current	0.0182
$\beta_{CapChR2}$	Scaling factor for CapChR2-mediated current	10^{-6}
τ_{Ca}	Time constant of the passive decay process	$12ms$
τ_*	Integration time constant	$278ms$
τ	Time constant	$70s$
γ_d	Depression rate	101.5
θ_d	Depression threshold	0.07
γ_p	Potentiation rate	216.2
θ_p	Potentiation threshold	0.085
V_m	Resting Membrane potential	-70 mV
$N_{NMDAtotal}$	Total number of NMDA receptors	20
$p_{NMDAopen}$	Single channel opening probability	0.5
σ_{NMDA}	SD of the gaussian noise added	3.3% of g_{NMDA}
$N_{VDCCtotal}$	Total number of VDCC channels	5
$p_{VDCCopen}$	Single channel opening probability	0.52
σ_{VDCC}	SD of the gaussian noise added	10% of g_{VDCC}

Table 3. Synaptic plasticity model parameters[29,30].

Data availability
Data is provided within the manuscript or supplementary information files.

Received: 26 September 2024; Accepted: 20 March 2025
Published online: 01 April 2025

References
1. Ma, H. et al. Excitation–transcription coupling, neuronal gene expression and synaptic plasticity. *Nat. Rev. Neurosci.* **24**(11), 672–692 (2023).
2. Südhof, T. C. Neurotransmitter release: The last millisecond in the life of a synaptic vesicle. *Neuron* **80**(3), 675–690 (2013).

3. Kennedy, M. B. Synaptic signaling in learning and memory. *Cold Spring Harbor Perspect. Biol.* **8**(2), a016824 (2016).
4. Jędrzejewska-Szmek, J., Dorman, D. B. & Blackwell, K. T. Making time and space for calcium control of neuron activity. *Curr. Opin. Neurobiol.* **83**, 102804 (2023).
5. Lepeta, K. et al. Synaptopathies: synaptic dysfunction in neurological disorders – A review from students to students. *J. Neurochem.* **138**(6), 785–805 (2016).
6. Emiliani, V. et al. Optogenetics for light control of biological systems. *Nat. Rev. Methods Primers* **2**(1), 55 (2022).
7. Bansal, A., Shikha, S. & Zhang, Y. Towards translational optogenetics. *Nat. Biomed. Eng.* **7**(4), 349–369 (2023).
8. Sahel, J. A. et al. Partial recovery of visual function in a blind patient after optogenetic therapy. *Nat. Med.* **27**(7), 1223–1229 (2021).
9. Lahore, R. G. F. et al. Calcium-permeable channelrhodopsins for the photocontrol of calcium signaling. *Nat. Commun.* **13**(1), 7844 (2022).
10. Rost, B. R., Schneider-Warme, F., Schmitz, D. & Hegemann, P. Optogenetic tools for subcellular applications in neuroscience. *Neuron* **96**(3), 572–603 (2017).
11. Nabavi, S. et al. Engineering a memory with LTD and LTP. *Nature* **511**(7509), 348–352 (2014).
12. Jeong, Y. et al. Synaptic plasticity-dependent competition rule influences memory formation. *Nat. Commun.* **12**(1), 3915 (2021).
13. Boyden, E. S., Zhang, F., Bamberg, E., Nagel, G. & Deisseroth, K. Millisecond-timescale, genetically targeted optical control of neural activity. *Nat. Neurosci.* **8**(9), 1263–1268 (2005).
14. Zhang, Y. P. & Oertner, T. G. Optical induction of synaptic plasticity using a light-sensitive channel. *Nat. Methods* **4**(2), 139–141 (2007).
15. Schoenenberger, P., Schärer, Y. P. Z. & Oertner, T. G. Channelrhodopsin as a tool to investigate synaptic transmission and plasticity. *Exp. Physiol.* **96**(1), 34–39 (2011).
16. Oldani, S. et al. SynaptoPAC, an optogenetic tool for induction of presynaptic plasticity. *J. Neurochem.* **156**(3), 324–336 (2021).
17. Kakegawa, W. et al. Optogenetic control of synaptic AMPA receptor endocytosis reveals roles of LTD in motor learning. *Neuron* **99**(5), 985–998 (2018).
18. Stefanescu, R. A., Shivakeshavan, R. G., Khargonekar, P. P. & Talathi, S. S. Computational modeling of channelrhodopsin-2 photocurrent characteristics in relation to neural signaling. *Bull. Math. Biol.* **75**, 2208–2240 (2013).
19. Williams, J. C. et al. Computational optogenetics: Empirically-derived voltage-and light-sensitive channelrhodopsin-2 model. *PLoS Comput. Biol.* **9**(9), e1003220 (2013).
20. Saran, S., Gupta, N. & Roy, S. Theoretical analysis of low-power fast optogenetic control of firing of Chronos-expressing neurons. *Neurophoton.* **5**(2), 025009–025009 (2018).
21. Gupta, N., Bansal, H. & Roy, S. Theoretical optimization of high-frequency optogenetic spiking of red-shifted very fast-Chrimson-expressing neurons. *Neurophoton.* **6**(2), 025002–025002 (2019).
22. Bansal, H., Gupta, N. & Roy, S. Comparison of low-power, high-frequency and temporally precise optogenetic inhibition of spiking in NpHR, eNpHR3. 0 and Jaws-expressing neurons. *Biomed. Phys. Eng. Express* **6**(4), 045011 (2020).
23. Bansal, H., Gupta, N. & Roy, S. Theoretical analysis of low-power bidirectional optogenetic control of high-frequency neural codes with single spike resolution. *Neuroscience* **449**, 165–188 (2020).
24. Bansal, H., Gupta, N. & Roy, S. Theoretical analysis of optogenetic spiking with ChRmine, bReaChES and CsChrimson-expressing neurons for retinal prostheses. *J. Neural Eng.* **18**(4), 0460b8 (2021).
25. Bansal, H., Pyari, G. & Roy, S. Co-expressing fast channelrhodopsin with step-function opsin overcomes spike failure due to photocurrent desensitization in optogenetics: A theoretical study. *J. Neural Eng.* **19**(2), 026032 (2022).
26. Pyari, G., Bansal, H. & Roy, S. Ultra-low power deep sustained optogenetic excitation of human ventricular cardiomyocytes with red-shifted opsins: A computational study. *J. Physiol.* **600**(21), 4653–4676 (2022).
27. Pyari, G., Bansal, H. & Roy, S. Optogenetically mediated large volume suppression and synchronized excitation of human ventricular cardiomyocytes. *Pflügers Archiv-Eur. J. Physiol.* **475**(12), 1479–1503 (2023).
28. Bansal, H., Pyari, G. & Roy, S. Theoretical prediction of broadband ambient light optogenetic vision restoration with ChRmine and its mutants. *Sci. Rep.* **14**(1), 11642 (2024).
29. Graupner, M. & Brunel, N. STDP in a bistable synapse model based on CaMKII and associated signaling pathways. *PLoS Comput. Biol.* **3**(11), e221 (2007).
30. Chindemi, G. et al. A calcium-based plasticity model for predicting long-term potentiation and depression in the neocortex. *Nat. Commun.* **13**(1), 3038 (2022).
31. Gauvain, G. et al. Optogenetic therapy: High spatiotemporal resolution and pattern discrimination compatible with vision restoration in non-human primates. *Commun. Biol.* **4**, 125 (2021).
32. Eria-Oliveira, A. S. et al. Hijacking of internal calcium dynamics by intracellularly residing viral rhodopsins. *Nat. Commun.* **15**(1), 65 (2024).
33. Malenka, R. C. & Bear, M. F. LTP and LTD: An embarrassment of riches. *Neuron* **44**(1), 5–21 (2004).
34. Nicoll, R. A. A brief history of long-term potentiation. *Neuron* **93**(2), 281–290 (2017).
35. Dan, Y. & Poo, M. M. Spike timing-dependent plasticity: from synapse to perception. *Physiol. Rev.* **86**(3), 1033–1048 (2006).
36. Buchanan, K. & Mellor, J. The activity requirements for spike timing-dependent plasticity in the hippocampus. *Front. Synaptic Neurosci.* **2**, 1361 (2010).
37. Feldman, D. E. The spike-timing dependence of plasticity. *Neuron* **75**(4), 556–571 (2012).
38. Bansal, H., Pyari, G. & Roy, S. Optogenetic generation of neural firing patterns with temporal shaping of light pulses. *Photonics* **10**(5), 571 (2023).
39. Shouval, H. Z., Wang, S. S. H. & Wittenberg, G. M. Spike timing dependent plasticity: a consequence of more fundamental learning rules. *Front. Comput. Neurosci.* **4**(19), (2010).
40. Mattis, J. et al. Principles for applying optogenetic tools derived from direct comparative analysis of microbial opsins. *Nat. Methods* **9**(2), 159–172 (2012).
41. Tønnesen, J., Katona, G., Rózsa, B. & Nägerl, U. V. Spine neck plasticity regulates compartmentalization of synapses. *Nat. Neurosci.* **17**(5), 678–685 (2014).
42. Holbro, N., Grunditz, Å., Wiegert, J. S. & Oertner, T. G. AMPA receptors gate spine Ca^{2+} transients and spike-timing-dependent potentiation. *PNAS* **107**(36), 15975–15980 (2010).
43. Harnett, M. T., Makara, J. K., Spruston, N., Kath, W. L. & Magee, J. C. Synaptic amplification by dendritic spines enhances input cooperativity. *Nature* **491**(7425), 599–602 (2012).
44. Froemke, R. C., Poo, M. M. & Dan, Y. Spike-timing-dependent synaptic plasticity depends on dendritic location. *Nature* **434**(7030), 221–225 (2005).
45. Cornejo, V. H., Ofer, N. & Yuste, R. Voltage compartmentalization in dendritic spines in vivo. *Science* **375**(6576), 82–86 (2022).
46. Adesnik, H. & Abdeladim, L. Probing neural codes with two-photon holographic optogenetics. *Nat. Neurosci.* **24**(10), 1356–1366 (2021).
47. Accanto, N. et al. A flexible two-photon fiberscope for fast activity imaging and precise optogenetic photostimulation of neurons in freely moving mice. *Neuron* **111**(2), 176–189 (2023).
48. Faini, G. et al. Ultrafast light targeting for high-throughput precise control of neuronal networks. *Nat. Commun.* **14**(1), 1888 (2023).
49. Kishi, K. E. et al. Structural basis for channel conduction in the pump-like channelrhodopsin ChRmine. *Cell* **185**, 672–689 (2022).

50. Chen, S. et al. Near-infrared deep brain stimulation via upconversion nanoparticle–mediated optogenetics. *Science* **359**, 679–684 (2018).
51. Papagiakoumou, E., Ronzitti, E. & Emiliani, V. Scanless two-photon excitation with temporal focusing. *Nat. Methods* **17**, 571–581 (2020).
52. Lohmann, C. & Kessels, H. W. The developmental stages of synaptic plasticity. *J. Physiol.* **592**(1), 13–31 (2014).
53. Deisseroth, K., Etkin, A. & Malenka, R. C. Optogenetics and the circuit dynamics of psychiatric disease. *JAMA* **313**(20), 2019–2020 (2015).
54. Govorunova, E. G., Sineshchekov, O. A. & Spudich, J. L. Three families of channelrhodopsins and their use in optogenetics. *Neurosci. Behav. Physiol.* **49**, 163–168 (2019).
55. Schneider, F., Grimm, C. & Hegemann, P. Biophysics of channelrhodopsin. *Annu. Rev. Biophys.* **44**, 167–186 (2015).
56. Roy, S., Singh, C. P. & Reddy, K. P. J. Generalized model for all-optical light modulation in bacteriorhodopsin. *J. Appl. Phys.* **90**(8), 3679–3688 (2001).
57. Roy, S., Kikukawa, T., Sharma, P. & Kamo, N. All-optical switching in pharaonis phoborhodopsin protein molecules. *IEEE Trans. Nanobiosci.* **5**(3), 178–187 (2006).
58. Roy, S. & Yadav, C. All-optical sub-ps switching and parallel logic gates with bacteriorhodopsin (BR) protein and BR-gold nanoparticles. *Laser Phys. Lett.* **11**(12), 125901 (2014).
59. Engelhard, C., Chizhov, I., Siebert, F. & Engelhard, M. Microbial halorhodopsins: Light-driven chloride pumps. *Chem. Rev.* **118**(21), 10629–10645 (2018).
60. Roy, S., Pyari, G., & Bansal, H. Theoretical analysis of low-power deep synergistic sono-optogenetic excitation of neurons by co-expressing light-sensitive and mechano-sensitive ion-channels. *Commun. Biol.* **8**, 379 (2025).
61. Evans, B. D., Jarvis, S., Schultz, S. R. & Nikolic, K. PyRhO: A multiscale optogenetics simulation platform. *Front. Neuroinf.* **10**, 8 (2016).
62. Graupner, M. & Brunel, N. Calcium-based plasticity model explains sensitivity of synaptic changes to spike pattern, rate, and dendritic location. *PNAS* **109**(10), 3991–3996 (2012).
63. Saudargiene, A., Cobb, S. & Graham, B. P. A computational study on plasticity during theta cycles at S chaffer collateral synapses on CA1 pyramidal cells in the hippocampus. *Hippocampus* **25**(2), 208–218 (2015).
64. Jahr, C. E. & Stevens, C. F. A quantitative description of NMDA receptor-channel kinetic behavior. *J. Neurosci.* **10**(6), 1830–1837 (1990).
65. Grunditz, Å., Holbro, N., Tian, L., Zuo, Y. & Oertner, T. G. Spine neck plasticity controls postsynaptic calcium signals through electrical compartmentalization. *J. Neurosci.* **28**(50), 13457–13466 (2008).
66. Dixit, N., Pyari, G., Bansal, H., & Roy, S. Theoretical analysis of low-power optogenetic control of synaptic plasticity with subcellular expression of CapChR2 at postsynaptic spine, Zenodo. https://doi.org/10.5281/zenodo.15011170. (2025).

Acknowledgements
The authors are grateful to Revered Professor Prem Saran Satsangi for his kind inspiration and encouragement.

Author contributions
S.R. and H.B. formulated the objectives. N.D. and G.P. carried out the simulations and prepared the draft. All authors reviewed the manuscript.

Funding
This work was supported by Department of Science and Technology, India [CRG/2021/005139 and MTR/2021/000742 to S.R.].

Declarations

Competing interests
The authors declare no competing interests.

Additional information
Supplementary Information The online version contains supplementary material available at https://doi.org/10.1038/s41598-025-95355-6.

Correspondence and requests for materials should be addressed to S.R.